GLOBAL BIOGEOCHEMICAL CYCLES, VOL. , NO. , PAGES 1–7,

# Mesoscale variability of sea surface $pCO_2$: What does it respond to?

A. Mahadevan

Department of Earth Sciences, Boston University, USA

M. Lévy

Laboratoire d'Océanographie Dynamique et de Climatologie, Institut Pierre Simon Laplace, Université de Paris VI, France

L. Mémery

Laboratoire des Sciences de l'Environnement Marin (LEMAR), Institut Universitaire Européen de la Mer (IUEM), Technopole Brest Iroise, France

**Abstract.** We examine the impact of meso- and submeso-scale oceanic processes on the distribution of sea surface $pCO_2$ to explain variability observed at length scales of order 10 km. We ask whether the large $pCO_2$ excursions (50–150 $\mu$-atm) that occur over 10–25 km of the sea surface could be induced by vertical advection associated with fronts and eddies in the pelagic ocean. A numerical model of a highly resolved, but idealized, mesoscale flow field is used to model the surface $pCO_2$ response to submeso-scale upwelling, taking in to account the effect of wind, heat flux and phytoplankton production. The effect of upwelled DIC on surface $pCO_2$ is largely offset by the lower temperature of the upwelled water and the consumption of DIC by phytoplankton that respond to the simultaneously upwelled nitrate in a nutrient-limited setting. Since an upwelling induced change in surface temperature, DIC or nitrate is proportional to the vertical gradient of these properties beneath the mixed layer, the relative change in surface $pCO_2$ is also dependent on the relative strengths of these gradients. We find that only small variations in surface $pCO_2$ ($\sim$ 10 $\mu$-atm) are induced by submeso-scale upwelling. The larger (50–150 $\mu$ atm) variations observed at small scales ($\sim$ 10 km) are therefore not a direct consequence of submeso-scale upwelling. Our results suggest that these surface $pCO_2$ differences are likely to have been generated at larger scales (by differential properties and levels of biological productivity) and cascaded to smaller scales by horizontal advection at the sea surface.

## 1. Introduction

The exchange of carbon dioxide ($CO_2$) between the atmosphere and ocean is driven by a difference in the partial pressures of $CO_2$ ($pCO_2$) across the air-sea interface. The gas flux depends largely on the magnitude of the partial pressure difference and the wind intensity. While atmospheric $pCO_2$ is fairly uniform and well-monitored, oceanic $pCO_2$ is variable in space and time, and poorly sampled. Present day global estimates of the air-sea $CO_2$ flux are based on a compilation of sea surface $pCO_2$ measurements into mean climatological monthly maps [*Takahashi et al.* [1997]; *Takahashi* [2002]; *Feely et al.* [2002]] that are used along with estimated wind speeds and an exchange coefficient formulation [*Wanninkhof* [1992]], to calculate monthly climatological air-sea fluxes of $CO_2$ at a global resolution of $4^0 \times 5^0$. While these estimates have brought us a long way in our search for a better quantification of the sources and sinks for atmospheric $CO_2$, there are still several questions and concerns about neglecting the smaller-scale variability in the $pCO_2$ and wind fields and the errors that might result as a consequence. Since $pCO_2$ is a nonlinear function of several variables, its value computed from a regional mean of the variables could be somewhat different than the mean regional $pCO_2$ [*Trela et al.* [1995]]. It is not clear whether sea surface $pCO_2$ is normally distributed and whether the climatological distributions of $pCO_2$ constructed by compositing several years of data appropriately represent the mean. Since the net global flux of carbon into the ocean is the small difference between a large in- and out-flux, it is sensitive to variability in either component. We thus have an interest in understanding and resolving the high degree of spatial and temporal variability occurring in surface $pCO_2$ and the resulting air-sea flux of $CO_2$.

It is known that surface $pCO_2$ can show significant seasonal [*Takahashi et al.* [1993]; *Bates et al.* [1998]; *Metzl et al.* [1995]], as well as interannual [*Bates* [2002]; *Feely et al.* [1999]; *Lefèvre et al.* [1999]] variability. But variability is also observed on shorter time scales ranging from days to weeks [*Taylor et al.* [1992]; *Hood et al.* [1999, 2001]] that are



Paper number .
0886-6236/03/$12.00

associated with *meso* (10–100 km) and *submeso* (1–10 km) length scale dynamics in the ocean. *Bates et al.* [2000] observe a spectral peak in the variability of sea surface $pCO_2$ and its temperature-adjusted value at mesoscales, suggesting that its variability is largely coupled to the dynamics. *Watson et al.* [1991] observed that in the late spring and early summer, sea surface $pCO_2$ in the North Atlantic was strongly modulated by biological activity, and that $pCO_2$, as well as the total dissolved inorganic carbon (DIC) were negatively correlated with chlorophyll. Variations of 5-10 $\mu$-atm across 10 km were common, but even variations as large as 70 $\mu$-atm were found to occur across tens of kilometers. In the Indian Ocean, *Metzl et al.* (personal communication) observed $pCO_2$ excursions of $\sim 150$ $\mu$-atm over tens of kilometers during the early summer. Here too, the DIC was strongly modulated by biology and showed strong anti-correlation with fluorescence. The Carioca buoy and POMME data [*N.R. Bates, L. Merlivat and L. Mémery* personal communication] from the North Atlantic are rife with smaller variations overlaid, sometimes, on a gradual trend. In these data sets, both temperature and DIC are seen to exert the dominant control on $pCO_2$ in different instances. A gradual increase in temperature is reflected in a corresponding rise the $pCO_2$, while large and abrupt DIC variations that result from phytoplankton blooms generate more dramatic $pCO_2$ variations.

This work is aimed at improving our understanding of the meso- and submeso-scale variability of $pCO_2$ and its controlling processes. It is motivated by the need to understand observations such as those described above. In particular, we aim to assess the role of mesoscale ocean dynamics on the sea surface $pCO_2$ variability. During spring bloom conditions, the vertical gradients of DIC, $NO_3$ and temperature are relatively weak or non-existent in the upper ocean, DIC, $NO_3$ and temperature are poorly correlated, nutrients are available at the surface, and the local consumption of DIC by phytoplankton can drive large $pCO_2$ variations. The large horizontal variability in $pCO_2$ that is generated in such situations is likely to cascade to smaller scales due to stirring by horizontal advection, as is shown for phytoplankton [*Abraham* [1998]; *Lévy* [2003]]. During oligotrophic conditions, on the other hand, the surface waters are generally depleted of nutrients, convective mixing is minimal, and there are strong vertical gradients in temperature, DIC and $NO_3$ just beneath the mixed layer. Under such conditions, meso- and submeso-scale upwelling associated with fronts and eddies in the ocean contribute significantly to the delivery of nutrients to the surface, thereby affecting the levels of new and primary production [*Lévy et al.* [2001]; *Mahadevan and Archer* [2000]; *McGillicuddy et al.* [1998]; *Flierl and McGillicuddy* [2002]; *Follows and Williams* [2003] and references therein]. Such upwelling can occur at scales smaller than the characteristic eddy scale (the internal Rossby radius of deformation) and hence introduce small-scale variance in the surface distributions [*Mahadevan and Campbell* [2002]]. It can significantly modulate not only the nutrients and biology in the surface ocean, but also temperature and DIC. The potential implications of these vertical fluxes on surface $pCO_2$ raises several questions. What magnitude of $pCO_2$ variations can potentially be induced by the dynamics? To what parameters are these variations most sensitive? Is meso- and submeso-scale vertical transport the major cause of surface $pCO_2$ variability and can it account for the large $pCO_2$ excursions that are observed over tens of kilometers? These are the sorts of issues that we intend to address through this study.

The $pCO_2$ of sea water varies largely with the temperature, T of the water, its DIC content, and total alkalinity, ALK. It increases non-linearly with T and DIC, but decreases with ALK. In general, DIC increases with depth in the ocean, while temperature decreases with depth. Hence, the upwelling of DIC from the sub-surface tends to increase sea surface $pCO_2$, but the lower temperature of the upwelled water counters this. In addition, the biological production of phytoplankton that is induced by the upwelling of nutrients (nitrate and phosphate) consumes DIC in the surface layer and draws down surface $pCO_2$. The change in surface T, DIC and ALK that is induced by upwelling is a function not only of the upwelling intensity, but also of the vertical gradients of these properties beneath the mixed layer, the mixed-layer depth and mixing efficiency. If we assume Redfied stochiometry, the DIC consumed by biological production at the surface is proportional to the nitrate ($NO_3$) upwelled, which in turn is related to the vertical gradient of the $NO_3$. Hence, for a given intensity of upwelling, the modulation in surface $pCO_2$ is dependent on the relative vertical gradients of T, DIC, ALK and $NO_3$. In the long run, the cumulative rate of vertical exchange affects the vertical gradients of these tracers in the ocean, but in this study, we merely examine the effect of localized vertical transport on surface $pCO_2$ as a function of the vertical gradients.

This study focuses on the effects of intermittent and small scale upwelling associated with fronts and eddies, rather than the persistent large-scale upwelling that is observed, for example, in the equatorial upwelling zones. When the upwelling is associated with a large-scale wind field, the divergence of the surface layer draws water up to surface over large areas. The deep mixed layer in the equatorial upwelling zones may also be a result of the strong shear due to the Equatorial undercurrent. The net result is that the upwelled DIC makes its expression at the surface. The heat flux, that also occurs on large scales, contributes to the warming of the DIC-rich upwelled waters and results in substantially elevating the surface $pCO_2$. Thus, the cumulative effect of heat flux and upwelling is important in the evolution of surface $pCO_2$ on the global scale, as for example, in the equatorial oceans. But, it is thought to be relatively less important in the case of sub-mesoscale upwelling for reasons explained in the section describing our results.

In what follows, we describe a modeling study to address the questions raised by observations of sea surface $pCO_2$. We use a high resolution three-dimensional ocean circulation model to simulate the dynamics of a meandering front with eddies and the associated vertical transport. A state of the art ecological model consisting of interactions between nitrate, phytoplankton, zooplankton, ammonia, detritus and dissolved organic matter is used to simulate the biological response in the upper ocean and its effect on the carbon and nitrogen chemistry of the water. We also model the mixed layer dynamics of the upper ocean which is forced with wind and heat fluxes. We initialize the T, DIC and $NO_3$ fields in the model based on commonly found values for the vertical gradients of these properties in the North Atlantic subtropical gyre. The sensitivity of the surface $pCO_2$ to upwelling depends on the ratios of the vertical gradients of T, DIC and $NO_3$. In the model, we attempt to maximize the $pCO_2$ variations by meso- and submeso-scale upwelling. Hence, we use initializations to favor this, as well as to isolate its effects from those of horizontal advection acting on different $pCO_2$ waters.

## 2. Modeling

### 2.1. Model Configuration

We use the OPA primitive equation ocean model from LODYC [*Madec et al.* [1999]] to simulate interactive mesoscale structures resulting from the nonlinear evolution of an unstable baroclinic front. Fronts are ubiquitous to the ocean and their meanders often develop into eddies, as is seen in our simulation. Hence we consider the evolving front and its associated structures to be a general representation of an energetic mesoscale flow field in the ocean. The model is set up in a channel-like domain 162 km in east-west extent, 486 km in north-south extent, and 4000 m deep, with solid north-south boundaries and periodic east-west boundaries. We treat density as a function of temperature alone; the salinity is uniform and constant. The upper layers of the southern half of the channel are warmer than the northern half and the mid-channel density is an interpolation of the northern and southern density profiles. The basic state is an east-west uniform potential vorticity zonal jet in geostrophic and hydrostatic balance. The jet-like flow is aligned with the contours of density on account of geostrophy. The mean density profile yields a first baroclinic Rossby radius of deformation of approximately 30 km. Details of the model and a physical description of the flow are in *Lévy et al.* [2001]. We use a model resolution of 2 km × 2 km in the horizontal plane in order to resolve the sub-mesoscale vertical velocities. In the vertical, the grid resolution varies. It is finer in the upper ocean, starting at 10m near the surface and gradually increasing to 300 m at depth.

The dynamical model is coupled to a biogeochemical model for nitrate, phytoplankton, zooplankton, ammonia, detritus, dissolved organic matter and DIC. The DIC is coupled in Redfield proportion to $NO_3$, which is the limiting nutrient. The parameters for the biological model are the same as in *Lévy et al.* [2001]. We experiment with and without the biological contribution and with different values of wind stress and net surface heat flux. Wind stress and a negative heat flux applied at the surface of the model induce mixing. The deepening of the mixed layer is also influenced by the density stratification and velocity shear. Since we are interested in mesoscale variations in sea-surface $pCO_2$ on a time scale of weeks and want to isolate the effect of vertical motion, we neglect the air-sea transfer of $CO_2$ which occurs over much longer time scales. It would take a 100m-deep mixed layer, for example, about a year to equilibrate its $pCO_2$ with the atmosphere by air-sea flux.

### 2.2. Model Parameters

The sensitivity of surface $pCO_2$ to meso- and submesoscale upwelling is largely a function of the ratio of the vertical gradients of T, DIC, ALK and $NO_3$ just beneath the mixed layer. This can be seen by expressing the change in $pCO_2$, $\Delta pCO_2$, in terms of the variations in T, DIC and ALK, viz. $\Delta$T, $\Delta$DIC, $\Delta$ALK, as [*Takahashi et al.* [1993]]

$$\Delta \mathrm{pCO_2} = \frac{\partial \mathrm{pCO_2}}{\partial \mathrm{T}} \Delta \mathrm{T} + \frac{\partial \mathrm{pCO_2}}{\partial \mathrm{DIC}} \Delta \mathrm{DIC} + \frac{\partial \mathrm{pCO_2}}{\partial \mathrm{ALK}} \Delta \mathrm{ALK}. \tag{1}$$

The relative change in $pCO_2$ to temperature, expressed as $\beta \equiv \frac{1}{\mathrm{pCO_2}} \frac{\partial \mathrm{pCO_2}}{\partial T}$, is fairly constant in the ocean [*Takahashi et al.* [1993]]. Using this definition of $\beta$, the Revelle factor $\xi \equiv \frac{\Delta \mathrm{pCO_2}}{\mathrm{pCO_2}} / \frac{\Delta \mathrm{DIC}}{\mathrm{DIC}}|_{\mathrm{ALK=const}}$, and its alkalinity equivalent $\xi_A \equiv \frac{\Delta \mathrm{pCO_2}}{\mathrm{pCO_2}} / \frac{\Delta \mathrm{ALK}}{\mathrm{ALK}}|_{\mathrm{DIC=const}}$, we can express the relative change in $pCO_2$ due to T, DIC and ALK variations as

$$\frac{\Delta \mathrm{pCO_2}}{\mathrm{pCO_2}} = \beta \Delta T + \xi \frac{\Delta \mathrm{DIC}}{\mathrm{DIC}} + \xi_A \frac{\Delta \mathrm{ALK}}{\mathrm{ALK}}. \tag{2}$$

The rate of change of a property, for example T, due to advection by a vertical velocity $w$ is given as $\frac{\partial T}{\partial t} = -w \frac{\partial T}{\partial z}$. Hence the relative change in surface $pCO_2$ in a time interval $\Delta t$ that is caused by upwelling can be be written as

$$\frac{\Delta \mathrm{pCO_2}}{\mathrm{pCO_2}} = -\frac{w \Delta t}{\Delta z} (\beta \Delta \mathrm{T}_z + \xi \frac{\Delta \mathrm{DIC}_z}{\mathrm{DIC}} + \xi_A \frac{\Delta \mathrm{ALK}_z}{\mathrm{ALK}}), \tag{3}$$

where $\Delta \mathrm{T}_z, \Delta \mathrm{DIC}_z, \Delta \mathrm{ALK}_z$ are the vertical variations in T, DIC and ALK occurring over a height $\Delta z$ just beneath the mixed layer. By denoting the ratios of the second and third terms in parenthesis to the first as

$$\gamma_C \equiv \frac{-\xi}{\beta\ \mathrm{DIC}} \frac{\Delta \mathrm{DIC}_z}{\Delta \mathrm{T}_z} \quad \text{and} \quad \gamma_A \equiv \frac{-\xi_A}{\beta\ \mathrm{ALK}} \frac{\Delta \mathrm{ALK}_z}{\Delta \mathrm{T}_z}, \tag{4}$$

the relative change in $pCO_2$ due to upwelling can be expressed as

$$\frac{\Delta \mathrm{pCO_2}}{\mathrm{pCO_2}} = -\frac{w \Delta t}{\Delta z} (1 - \gamma) \beta \Delta_z \mathrm{T}, \quad \text{where } \gamma = \gamma_C + \gamma_A. \tag{5}$$

In most regions of the ocean, the vertical gradients of ALK are weak as compared to those of DIC, i.e., $|\gamma_A| < |\gamma_C|$. Alkalinity and salinity are held constant in this model for simplicity and effectively $\gamma = \gamma_C$. Alternatively, the DIC in the model can be interpreted as a combination of the DIC and ALK in the ocean, so that henceforth we use only one parameter $\gamma$ (rather than $\gamma_C$ and $\gamma_A$) and one variable, viz. DIC (instead of DIC and ALK). Temperature and DIC are generally negatively correlated in the ocean, so that $\Delta \mathrm{DIC}_z / \Delta \mathrm{T}_z < 0$ and $\gamma > 0$. If $\gamma = 1$, it means that upwelling has no effect on surface $pCO_2$, because the effect of DIC and temperature, cancel each other. If, on the other hand, $\gamma > 1$, the surface $pCO_2$ is increased by upwelling, and if $\gamma < 1$, the $pCO_2$ is decreased by upwelling. This is the case when no biological consumption of DIC is considered.

In a nutrient limited setting, the DIC consumed by phytoplankton in a time interval $\Delta t$ in response to a submesoscale upwelling velocity $w$ is denoted by $\Delta_{\mathrm{bio}}\mathrm{DIC}$ and estimated as the upwelled $NO_3$ times the Redfield ratio $R_{C:N}$, i.e., $-\frac{w \Delta t}{\Delta z}\ \Delta \mathrm{NO}_{3z}\ R_{C:N}$, where $\mathrm{NO}_{3z}/\Delta z$ is the vertical gradient of nitrate beneath the mixed layer. Expressing the ratio of the DIC consumed by phytoplankton to the the upwelled DIC as

$$\delta = R_{C:N}\ \frac{\Delta \mathrm{NO}_{3z}}{\Delta \mathrm{DIC}_z}, \tag{6}$$

we can express the biological uptake of DIC resulting from the vertical nitrate flux as

$$\Delta_{\mathrm{bio}}\mathrm{DIC} = -\frac{w \Delta t}{\Delta z}\ \delta\ \Delta \mathrm{DIC}_z. \tag{7}$$

This must be deducted from the upwelled DIC, resulting in the relative change in $pCO_2$ to be modified as

$$\frac{\Delta \mathrm{pCO_2}}{\mathrm{pCO_2}} = -\frac{w \Delta t}{\Delta z} (1 - \Gamma)\ \beta\ \Delta \mathrm{T}_z, \quad \text{where } \Gamma = \gamma(1 - \delta) \tag{8}$$

The parameter $\Gamma$ takes in to account the effect of biological productivity. When $\Gamma = 1$, vertical transport has no net effect on the surface $pCO_2$ after accounting for biological consumption, but when $\Gamma > 1$ or $< 1$, one can expect localized upwelling to increase, or respectively, decrease surface $pCO_2$.

### 2.3. Model Initialization

We initialize the model domain with an across-channel front in temperature (Fig. 1) as in *Lévy et al.* [2001]. To initialize the DIC we choose a value for $\gamma$ to characterize the correlation between DIC and T in the vertical. An analogous parameter $\gamma_s$ is used to relate DIC and T at the sea surface. The idea is that by setting $\gamma_s = 1$, the sea surface $pCO_2$ can be made uniform even when $\gamma \neq 1$. Further, the relationship between DIC and T is likely to be different at the sea surface than at depth because of air-sea gas exchange, heat fluxes and biological activity. To initialize the model DIC as a function of the T field we prescribe a value of DIC at any one point in the surface layer of the model. The DIC at any neighboring location varies from the initial location by $\Delta\mathrm{DIC} = -\beta\,\mathrm{DIC}\,\gamma^*\,\Delta\mathrm{T}/\xi$ in accordance with (4), where $\Delta$T is the temperature variation between the two locations and $\xi$ is evaluated at the new location. The parameter $\gamma^*$ takes the values $\gamma_s$ at the surface, but changes to $\gamma$ at depth to generate vertical gradients in the desired ratio. It is evaluated as $\gamma^* = \gamma_s \exp(-z/z_m) + \gamma(1 - \exp(-z/z_m))$, where $z$ is the depth below the mixed layer, and $z_m$ is taken to be 50m. Using such a blending function ensures that the DIC varies smoothly on isopycnals that are exposed to the surface on one side of the front, but lie subsurface and have a different DIC value on the other side. Choosing $\gamma_s$, $\gamma$, and the value of DIC at any one point at the surface thus defines the DIC distribution in terms of T over the entire domain. The initial T and DIC fields are shown in Fig. 2 when $\gamma_s = 1$ and $\gamma = 4$. When $\gamma_s = 1$, the meridional change in T at the surface is compensated by the change in DIC; this is representative of a situation in which the sea surface $pCO_2$ is perfectly equilibrated with the atmosphere. We use $\gamma_s = 1$ to isolate the effect of vertical advection on surface $pCO_2$ from that of horizontal advection. Using coarsely gridded global estimates of the mean climatological DIC, ALK and T distributions, we estimated the value $\gamma$ for the world's oceans [manuscript in preparation]. It was found that $\gamma$ lies in the range 1–2 for about 50% of the world's oceans, 2–3 for 15–20% of the ocean, and 3–5 for 5–10% of the ocean. We take $\gamma$ to be 4 to simulate conditions in which the surface $pCO_2$ is sensitive to upwelling.

In the model runs with biology, we need to initialize the nitrate field. We set the initial $NO_3$ concentration to 0 above the nutricline, which we set at 100 m to mimic summer-like conditions in which productivity is limited by the vertical advective supply of nutrients occurring at submesocales. Beneath the nutricline, we relate $NO_3$ to DIC by choosing a value of $\delta$ and and thereby prescribing the vertical $NO_3$ gradient in accordance with (6). $R_{C:N}$ is taken to be 6.625. We run each model simulation with the same initial temperature and velocity fields, but can vary the initial DIC and $NO_3$ distributions by changing $\gamma, \gamma_s$ and $\delta$.

### 2.4. Numerics

All the variables in the model, T, DIC, $NO_3$, phytoplankton, zooplankton, ammonia, detritus, and dissolved organic matter, are advected by the flow field. We find that spurious values of $pCO_2$ can be generated by using different numerical advection algorithms (or different time steps, eddy viscosity coefficients, or convective adjustment) for DIC and T, the variables on which $pCO_2$ is dependent. Since the distributions of DIC and T are negatively correlated, i.e., an increase in one is generally associated with a decrease in the other, and $pCO_2$ increases non-linearly with each of them, a discrepancy in the rates of propagation of DIC and T can lead to exceptionally large excursions in $pCO_2$. This particularly stands out at the frontal outcrop when the domain is initialized with large, but negatively correlated variations in DIC and T across the front that generate a uniform $pCO_2$ field throughout the domain ($\gamma = \gamma_s = 1$). To avoid such errors, we have used the same numerics for all the variables. Since the Arakawa scheme is used for the advection of temperature [*Madec et al.* [1999]], we use the same for all the other variables.

## 3. Results

### 3.1. Dynamical Processes

The model is started from a geostrophically balanced state. The front that separates warm surface water in the southern half of the channel from cooler water in the north is associated with an east-west jet in the upper ocean. The front is baroclinically unstable and the weak initial meander introduced as a perturbation to the front, grows as the simulation progresses. The meandering grows until eddies are pinched off, and the across-front mixing caused in this way leads to the gradual decay of the front. Results shown and discussed here are only for the first month of the simulation which entails meander growth and eddy pinch-off. The general evolution of the sea surface temperature (SST) pattern is for this period is shown in Fig. 2.

Deviations from geostrophic balance arising, for example, from the growth of instabilities can lead to non-divergent horizontal velocities and to upwelling and subduction that occurs largely along sloping isopycnal surfaces. These vertical velocities occur in narrow regions and are closely associated with strong vorticity gradients characteristic of frontogenesis [*Woods* [1988]; *Pollard and Regier* [1992]; *Shearman et al.* [1999]]. The magnitude of the vertical velocities is sensitive to the horizontal spatial resolution in the numerical model. Resolving the strong vorticity gradients and the associated dynamics at the filament scale is essential for capturing the vertical transport correctly [*Lévy et al.* [2001]]. Water that is upwelled isopycnally to the base of the mixed layer is then conveyed to the surface by vertical mixing that is induced by buoyancy and momentum fluxes at the surface. Sea surface DIC and $pCO_2$ are therefore sensitive to the intensity of mixing and hence to the intensity and intermittency of the wind stress [*Bates and Merlivat* [2001]; *Mémery et al.* [2002]]. Our model simulations generate upwelling advective velocities in the range of 10 to 50 meters per day at an approximate depth of 100 m [*Lévy et al.* [2001]]. This is typical of fairly energetic eddies and fronts in the ocean. We impose a uniform surface wind stress of 0.3 dyne-cm$^{-2}$ to induce a reasonable level of mixing and maintain an average mixed layer depth of about 60 m. Without this wind-induced mixing, the signal of upwelling is not detectable at the surface. Fig. 4 shows a vertical across-front section through the upper 120m of the model domain. The dynamical uplift of DIC and cold

water is seen in the upper thermocline, while the effect of vertical mixing in conveying these signals to the surface is seen in the upper 50 meters or so. $NO_3$ is also uplifted into the euphotic layer along with DIC and a maximum in phytoplankton is generated at a depth of 40–50 m where light and nutrients are best optimized.

### 3.2. Competing Effects of Vertical Advection on Surface T and DIC

When the model is initialized with uniform $pCO_2$ in the surface mixed layer ($\gamma_s = 1$), variations in surface $pCO_2$ can be attributed to upwelling. The magnitude of the $pCO_2$ variations is dependent on the value of $\gamma$ in the absence of biological production and heat flux. When $\gamma = 1$, the effect of T and DIC variations induced by upwelling compensate each other, and the surface $pCO_2$ remains unchanged. As $\gamma$ is increased in the model, one detects a greater increase in surface $pCO_2$ with time in regions where upwelling enhances the DIC. Fig. 4b shows the surface $pCO_2$ after one month, in a model simulation performed without phytoplankton and initialized with $\gamma = 4$ and $\gamma_s = 1$. The $pCO_2$ is enhanced by approximately 10 $\mu$-atm in narrow regions that occupy a small percentage of the total surface area. These conditions in the model, viz. reasonably strong vertical velocities, an active mixed layer, and a value of $\gamma$ that is large compared to most of the oceans, favor the enhancement of surface $pCO_2$ by upwelling. An enhancement in these conditions can increase the observed variation in surface $pCO_2$, but only by a factor of two or three. An increased wind stress of 1 dyne-cm$^{-2}$, for example, further increases the surface $pCO_2$ maxima shown in Fig. 4b by about 10 $\mu$-atm. The magnitude of $pCO_2$ variations generated by submeso–scale upwelling seems to remain in the range of 10–20 $\mu$-atm for the experiments without biology.

### 3.3. Effect of Surface Heat Fluxes

When warmed, surface water becomes buoyant and isolated from the subsurface due to its strengthened stratification. This inhibits vertical mixing; the heat flux is distributed over a small depth and surface $pCO_2$ can rise rapidly and substantially. In the idealized configuration of our model, the upwelled waters do not reach the surface during such times, and the subsurface DIC gradient and value of $\gamma$ have little effect on the change in sea surface $pCO_2$. Small-scale spatial variability in $pCO_2$ is obliterated since the warming is large scale and not restricted to the upwellnig sites. In the model, we account for only the radiative heat flux, but neglect the latent and sensible heat fluxes. The surface temperature increases by an amount proportional to the heat flux and inversely proportional to the depth of heating. The change in temperature $\Delta T$ induced by a heat flux $Q$ in the mixed layer over a time interval $\Delta t$ can be quantified as $\Delta T = Q\Delta t/C_p H$, where $C_p$ is the specific heat capacity of the water and $H$ is the mixed layer depth. The relative change in $pCO_2$ due to a heat flux (HF) can be written as $\frac{\Delta pCO_2}{pCO_2}|_{HF} = \beta Q \Delta t/C_p H$ and its ratio to the term in (3) that quantifies the relative change in $pCO_2$ due to the effect of upwelling on temperature is $Q/C_p H w(\Delta T_z/\Delta z)$. The variability in the heat flux $Q$ is negligible at mesoscales and $C_p$ is nearly constant. However, $w, H$ and $\Delta T_z/\Delta z$ can vary at these scales. At the locations where submesoscale upwelling occurs, $w$ is much larger than in surrounding regions and hence the relative effect of heat flux, as compared to upwelling, is smaller at the upwelling locations than in the surrounding waters. For these reasons, the effect of surface warming in conjunction with upwelling of DIC is relatively insignificant in our model simulations of sub-mesoscale upwelling. We see no significant further enhancement in $pCO_2$ by heat fluxes at the upwelling locations, as is known to occur in regions of large-scale upwelling. It is not clear whether this is entirely true in the oceans or whether the model's finding is affected by its limitations in handling the heat fluxes, mixed layer dynamics and air-sea interaction.

Cooling destabilizes and mixes the water column, results in the deepening of the mixed layer by entrainment, and a loss of heat over the depth of the mixed layer. Regions where the mixed layer deepens rapidly experience relatively less change in sea surface $pCO_2$ due to the temperature effect, as compared to regions where the cooling is restricted to occurs over a small depth. The depth of the mixed layer in the model shows considerable variability on mesoscales, as in other studies [*Nurser and Zhang* [2000]; *Lévy et al.* [2000]], and the variation of surface $pCO_2$ induced by cooling is linked to the variability in the mixed layer structure. In the model we observe that the mixed layer is shallowest at fronts, around eddies, and in filaments, where the isopycnals are steeply sloping. These are the regions where surface $pCO_2$ is lowered the most by cooling (Fig. 4c). While the surface temperature decreases, surface DIC is enhanced by the deepening of the mixed-layer and entrainment of DIC-rich water from the subsurface. The modulation of surface DIC and $pCO_2$ is thus dependent on the vertical DIC gradient (i.e., the value of $\gamma$) and the depth of entrainment. For a given heat loss and density distribution, higher values of $\gamma$ imply a lessor drop in sea-surface $pCO_2$. The model simulations performed with $\gamma = 4$ and a uniform heat loss of 50 watts-m$^2$ resulted in surface $pCO_2$ variations of approximately 11 $\mu$-atm after a month. This results indicate that small scale variability in surface $pCO_2$ is decreased by heating and increased by cooling.

### 3.4. Effect of Biology

A net uptake of DIC by biological production in the upper ocean tends to lower the surface $pCO_2$. At times when surface waters become abundant in nutrient, phytoplankton blooms occur, and can draw down sea surface $pCO_2$ by as much as 50–100 $\mu$-atm [*Taylor et al.* [1992]]. At other times, particularly in subtropical gyre centers, productivity is largely limited by the the supply of nutrients. In our model simulations initialized with a nutricline at 100 m (to reflect an oligotrophic setting like that of the subtropical gyres in the late summer), new production is limited to regions where the nutrients are uplifted into the euphotic zone. This occurs in the same locations where the DIC is enhanced due to a flux from the subsurface. The uptake of DIC by phytoplankton thus curtails the enhancement of $pCO_2$ resulting from DIC upwelling (Fig. 3d and 4d). The regions of intense upwelling are where isopycnals are sloping upward and outcropping. In the model, mixing is limited to shallow depths at such sites and the DIC modulation is visible at the surface. Under such conditions, the changes in DIC and $pCO_2$ are sensitive to the values of $\delta$ and $\Gamma$. For a value of $\gamma = 4$, we used $\delta = 0.6, 0.75$, and 0.9, resulting in $\Gamma = 1.6, 1$ and 0.4, respectively. These values span a large part of the range of values for $\delta$ and $\Gamma$ estimated

from global climatological distributions of $NO_3$, DIC, ALK and T [manuscript in preparation]. When $\Gamma = 1$, upwelling has little effect on surface $pCO_2$; when $\Gamma < 1$, surface $pCO_2$ is lowered by upwelling because the effects of the lowered temperature and DIC consumption outweigh the effect of upwelled DIC. Similarly, when $\Gamma > 1$, $pCO_2$ is increased because of a surfeit of DIC at the surface. Using a value of $\Gamma = 0.4$ (which is fairly extreme for most of the oceans and should hence maximize the variations that might be generated in surface $pCO_2$ by upwelling) results in localized reductions in the surface $pCO_2$ of only about 7 $\mu$-atm in a month's time.

### 3.5. Effect of Horizontal Advection

The pCO2 of the surface ocean is much more variable than that of the atmosphere because the atmosphere is well-mixed. The surface ocean equilibrates with the atmosphere very slowly (on a time scale $\sim$ 1 year) as compared to the time scales on which it is disturbed from equilibrium by upwelling, mixing, heat flux and biological production ($\sim$ days to weeks). It is typical to find different water masses in the surface ocean that differ in their properties, rates of biological productivity and $pCO_2$. Water on one side of a front, for example, can be in greater communication with the subsurface and hence differ from the other side. If we initialize our model with a different surface $pCO_2$ on either side of the front ($\gamma_s \neq 1$), the evolution of the surface $pCO_2$ field is dominated by the lateral advection and stirring of the different $pCO_2$ surface waters and the impact of upwelling is indiscernible (Fig. 5). This suggests that mesoscale activity influences sea surface $pCO_2$ not so much by sub-mesoscale vertical transport that is crucial for nutrient supply, but rather by the horizontal advection of surface $pCO_2$ differences. Such $pCO_2$ differences are generated over larger spatial and temporal scales than those associated with sub-mesoscale upwelling. But meso and submeso scale filaments of $pCO_2$ variations are generated by the horizontal stirring of the different $pCO_2$ waters. The range of variability in surface $pCO_2$ values is determined by the properties and large scale $pCO_2$ differences of the surface water masses that are stirred and is much larger than the variability induced by vertical fluxes alone.

## 4. Conclusions

The variation in surface $pCO_2$ that can be induced by meso- and submeso-scale vertical transport is dependent on the ratio of the vertical gradients of DIC and ALK to T (and in addition $NO_3$ to DIC when biological productivity is considered, but is nutrient-limited) just beneath the mixed layer. Surface $pCO_2$ increases or decreases in response to submeso-scale upwelling according as $\Gamma > 1$ or $< 1$. The magnitude of the $pCO_2$ modulations depend the magnitude of $1 - \Gamma$, the upwelling velocities, and the strength of wind- and cooling-induced mixing. The surface $pCO_2$ variations in response to submeso-scale upwelling occur in frontal regions where vertical motion is pronounced. The DIC is elevated due to upwelling in such regions, but the simultaneous supply of nitrate fuels new production which consequently draws down the DIC. Warming increases sea surface $pCO_2$ rapidly and fairly uniformly over the region because stratification isolates the surface from below. The change in surface $pCO_2$ that results from cooling on the other hand, is variable and depends on the mixed layer structure and depth of mixing, the entrainment of DIC and $NO_3$, and the biological consequences. Even though we initialize the DIC and $NO_3$ in our model to favor the response of surface $pCO_2$ to upwelling, we find that reasonably intense submeso-scale upwelling of 10–50 m-day$^{-1}$ and fairly active mixing generated by a surface wind stress of 0.3 dynes cm$^{-2}$, induces surface $pCO_2$ variations of only about 10 $\mu$-atm in a month's time. An increase in the mixing rate or length of simulation can somewhat increase these numbers, but they remain much smaller than the large $pCO_2$ variations ($\sim$ 100 $\mu$-atm) that have been observed in the surface ocean over tens of kilometers. Large surface $pCO_2$ differences ($\sim$ 100 $\mu$-atm) can occur across different water masses and fronts and when intense phytoplankton blooms draw down the DIC over certain regions, but are typically generated over larger scales than the meso and submeso scale. Our experiments suggest that the cascade of this large scale surface $pCO_2$ variance to smaller scales that occurs through horizontal advection and stirring (while preserving the magnitude of the variations) is manifest as large $pCO_2$ excursions at small scales. The variations in surface $pCO_2$ generated by meso- and submesoscale vertical transport are much smaller ($\sim 10\mu$-atm). These findings seem to be consistent with observations [e.g. Wanninkhof and Feely ,NOAA Global Carbon Cycle data pub. page 167 *LSCOP* [2002], Carioca (Bates et al. pers. comm), Southern Indian ocean (Metzl et al. pers. comm)].

**Acknowledgments.** This work was supported by CNRS, IDRIS and NASA (NAG5-11258). AM thanks LODYC and CNRS for hosting her stay in Paris, and S. Emerson and L. Merlivat for stimulating discussions.

## References

Abraham, E., The generation of plankton patchiness by turbulent stirring, *Nature*, *391*, 577–580, 1998.

Bates, N., Interannual variability the global ocean uptake of $CO_2$, *Geophysical Research Letters*, 2002.

Bates, N., and L. Merlivat, The effect of short-term wind variability on air-sea $CO_2$ exchange, *Geophysical Research Letters*, *28*, 3281–3284, 2001.

Bates, N., T. Takahashi, D. Chipman, and A. Knap, Variability of $pCO_2$ on diel to seasonal timescales in the Sargasso Sea, *Journal of Geophysical Research*, *103*, 15,567–15,585, 1998.

Bates, N., L. Merlivat, L. Beaumont, and A. Pequignet, Intercomparison of shipboard and moored CARIOCA buoy seawater $fCO_2$ measurements in the Sargasso Sea, *Marine Chemistry*, *72*, 239–255, 2000.

Feely, R., R. Wanninkhof, T. Takahashi, and P. Tans, Influence of El Niño on the equatorial Pacific contribution to atmospheric $CO_2$ accumulation, *Nature*, *398*, 597–601, 1999.

Feely, R., C. Sabine, T. Takahashi, and R. Wanninkhof, Uptake and storage of carbon dioxide in the ocean: The global $CO_2$ survey, *Oceanography*, *14*, 25–32, 2002.

Flierl, G., and D. McGillicuddy, Mesocale and submesoscale physical-biological interactions in the sea, in *The Sea (Biological Physical Interactions in the Sea)*, edited by A. Robinson, J. McCarthy, and B. Rotschild, vol. 12, pp. 113–185, John Wiley & Sons, Inc. NY, 2002.

Follows, M., and R. Williams, Physical transport of nutrients and the maintenance of biological production, in *Ocean Biogeochemistry*, edited by M. Fasham, pp. 19–51, Springer-Verlag, 2003.

Hood, E., L. Merlivat, and T. Johannessen, Variations of $fCO_2$ and air-sea flux of $CO_2$ in the Greenland Sea gyre using high-frequency time series data from CARIOCA drift buoys, *Journal of Geophysical Research*, *104*, 20,571–20,583, 1999.

Hood, E., R. Wanninkhof, and L. Merlivat, Short timescale variations of $fCO_2$ in a North Atlantic warm-core eddy: Results from the Gas-Ex 98 carbon interface ocean atmosphere (CARIOCA) buoy data, *Journal of Geophysical Research*, *106*, 2561–2572, 2001.

Lefèvre, N., A. Watson, D. Cooper, R. Weiss, T. Takahashi, and S. C. Sutherland, Assessing the seasonality of the oceanic sink for $CO_2$ in the northern hemisphere, *Global Biogeochemical Cycles*, *13*, 273–286, 1999.

Lévy, M., Mesoscale variability of phytoplankton and of new production: Impact of the large-scale nutrient distribution, *Journal of Geophysical Research (in review)*, 2003.

Lévy, M., L. Mémery, and G. Madec, Combined effects of mesoscale processes and atmospheric high-frequency variability on the spring bloom in the MEDOC area, *Deep-Sea Research*, *47*, 27–53 doi:10.1016/S0967–0637(99)00,051–5, 2000.

Lévy, M., P. Klein, and A.-M. Treguier, Impacts of sub-mesoscale physics on production and subduction of phytoplankton in an oligotrophic regime, *Journal of Marine Research*, *59*, 535–565, 2001.

LSCOP, *A Large Scale $CO_2$ observing plan: In situ oceans and atmosphere*, NOAA, Office of Global Programs, 2002.

Madec, G., P. Delecluse, and M. I. adn C. Levy, OPA 8.1 Ocean General Circulation Model Reference Manual, *Tech. rep.*, Institut Pierre-Simon Laplace, 1999.

Mahadevan, A., and D. Archer, Modeling the impact of fronts and mesoscale circulation on the nutrient supply and biogeochemistry of the upper ocean, *Journal of Geophysical Research*, *105*, 1209–1225, 2000.

Mahadevan, A., and J. Campbell, Biogeochemical patchiness at the sea surface, *Geophysical Research Letters*, *29*, 1926, doi:10.10292001GL014,116, 2002.

McGillicuddy, D., Jr., A. Robinson, D. Siegel, H. Jannasch, R. Johnson, T. Dickey, J. McNeil, A. Michaels, and A. Knap, Influence of mesoscale eddies on new production in the Sargasso Sea, *Nature*, *394*, 263–266, 1998.

Mémery, L., M. Lévy, S. Vérant, and L. Merlivat, The relevant time scales in estimating the air-sea $CO_2$ exchange in a mid-latitude region, *Deep Sea Research II*, *49*, 2067–2092, 2002.

Metzl, N., A. Poisson, F. Louanchi, C. Brunet, B. Schauer, and B. Bres, Spatio-temporal distributions of air-sea fluxes of $CO_2$ in the Indian and Antarctic oceans, *Tellus*, *47B*, 56–69, 1995.

Nurser, A., and J. Zhang, Eddy-induced mixed layer shallowing and mixed layer thermocline exchange, *Journal of Geophysical Research*, *105*, 21,851–21,868, 2000.

Pollard, R., and L. Regier, Vorticity and vertical circulation at an ocean front, *Journal of Physical Oceanography*, *22*, 609–625, 1992.

Shearman, R., J. Barth, and P. Kosro, Diagnosis of three-dimensional circulation associated with mesoscale motion in the California current, *Journal of Physical Oceanography*, *29*, 651–670, 1999.

Takahashi, T., Global sea-air $CO_2$ flux based on climatological surface ocean $pCO_2$, and seasonal biological and temperature effects, *Deep Sea Research Part II*, *49*, 1601–1622, 2002.

Takahashi, T., J. Olafsson, J. Goddard, D. Chipman, and S. C. Sutherland, Seasonal variation of $CO_2$ and nutrients in the high-latitude surface oceans: A comparative study, *Global Biogeochemical Cycles*, *7*, 843–878, 1993.

Takahashi, T., R. Feely, R. Weiss, R. Wanninkhoff, D. Chipman, S. Sutherland, and T. Takahashi, Global air-sea flux of $CO_2$: An estimate based on measurements of sea-air $pCO_2$ difference, *Proceedings of the National Academy of Sciences, USA*, *94*, 8292–8299, 1997.

Taylor, A., A. Watson, and J. E. Robertson, The influence of the spring phytoplankton bloom on carbon dioxide and oxygen concentrations in the surface waters of the northeast Atlantic during 1989, *Deep Sea Research*, *39*, 137–152, 1992.

Trela, P., S. Sathyendranath, R. Moore, and D. Kelley, Effect of the nonlinearity of the carbonate system on partial pressure of carbon dioxide in the oceans, *Journal of Geophysical Research*, *100*, 6829–6844, 1995.

Wanninkhof, R., Relationship between wind speed and gas exchange over the ocean, *Journal of Geophysical Research*, *97*, 7373–7382, 1992.

Watson, A., C. Robinson, J. Robinson, P. Ie, B. Williams, and M. Fasham, Spatial variability in the sink for atmospheric carbon dioxide in the North Atlantic, *Nature*, *350*, 50–53, 1991.

Woods, J., Mesoscale upwelling and primary production, in *Toward a Theory on Biological-Physical Interactions in the World Ocean*, edited by B. Rothschild, pp. 7–38, Kluwer Academic Publishers, 1988.

A. Mahadevan, Department of Earth Sciences, Boston University, 685 Commonwealth Avenue, Boston, MA 02215 (amala@bu.edu)

M. Lévy, Laboratoire d'Oceanographie Dynamique et de Climatologie, Institut Pierre Simon Laplace, Universite de Paris VI, France (levy@lodyc.jussieu.fr)

L. Mémery, Laboratoire des Sciences de l'Environnement Marin (LEMAR), Institut Universitaire Europen de la Mer (IUEM), Technopole Brest Iroise, Place Nicolas Copernic, 29820 Plouzan, France (memery@univ-brest.fr)

(Received June 2002.)

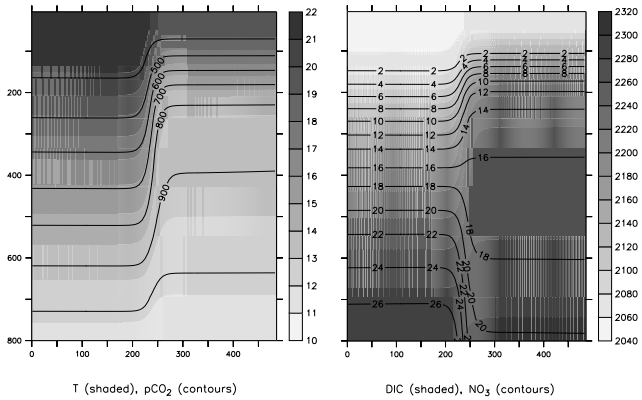


**Figure 1.** Initial distributions of T, DIC, $NO_3$ and $pCO_2$ along a mid-channel north-south cross-section that shows the upper 800 m of the domain. The $pCO_2$ is evaluated at atmospheric pressure. The horizontal axis is labeled in km and vertical axis in m. The north-south boundaries are impervious. In this initialization we used $\gamma = 4, \gamma_s = 1$, and $\delta = 0.75$ which results in $\Gamma = 1$. The north-south $NO_3$ gradient reverses sign at depth because the vertical gradients are weak at depth on the north side of the channel. The profiles of DIC, T and $NO_3$ are representative of the ocean in the upper 500 m; the distributions at depth are hardly of relevance to the model results.

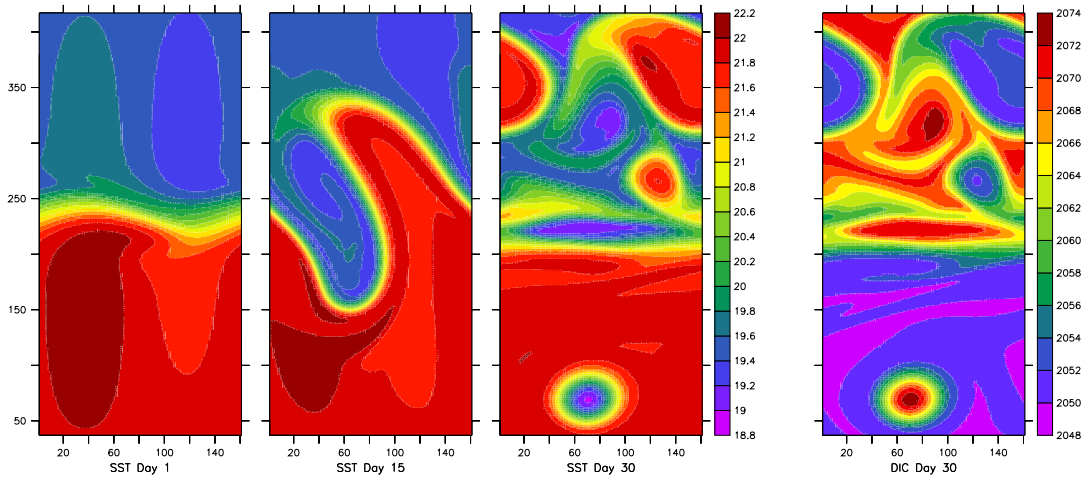


**Figure 2.** The first three plots show consecutive views of the model sea surface temperture show the development of the front and mesoscale structures over a month. The last plot shows the surface DIC on day 30 of the simulation; it was initialized with $\gamma_s = 1$ and is negatively correlated with temperature. The lateral boundaries are vertical; north-south boundaries are impervious, while east-west boundaries are periodic. An east-west wind stress of 0.3 dyne-cm$^{-2}$ is imposed at the surface in this simulation. No net heat flux is prescribed here. The axes are labeled in kilometers. With an east-west wind stress, up- and down-welling is generated near the north and south boundaries. These regions are eliminated from these and all other plots.

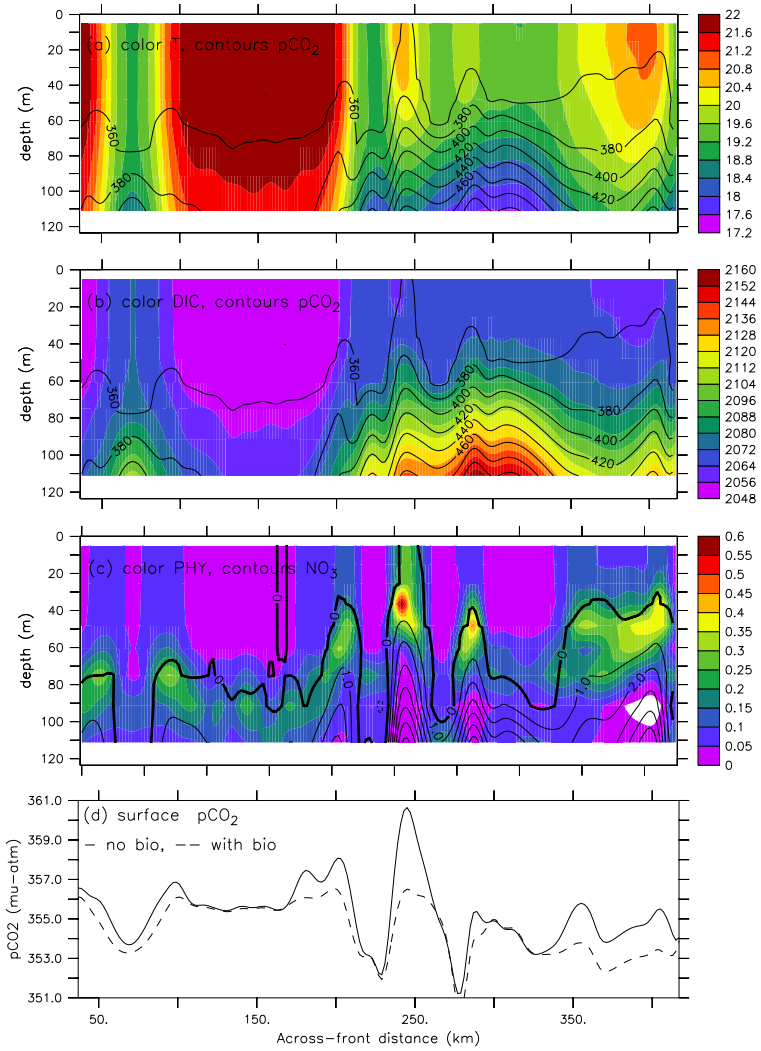


**Figure 3.** A north-south across-front section at x = 80 km (approximately mid-channel) showing (a) DIC and (b) temperature overlaid with contours of $pCO_2$ evaluated at atmospheric pressure. These fields are from day 30 of a model run initialized with $\gamma = 4$, $\gamma_s = 1$, constant ALK and salinity, and forced with an east-west wind stress of 0.3 dyne-cm$^{-2}$. The DIC is negatively correlated with T. There is no net heat flux and no biology in figures (a) and (b). DIC and cold water from the subsurface are upwelled and mixing vertically homogenizes the mixed layer conveying the upwelled water to the surface. When the wind stress is increased, the highs and lows in surface $pCO_2$ are more pronounced as increased mixing conveys a greater amount of upwelled DIC to the surface. In (c) we show the phytoplankton concentration overlaid with contours of nitrate. Since nitrate is upwelled along with DIC, phytoplankton is concentrated at the sites of upwelling. It draws down the DIC and the $pCO_2$ as seen in (d) in the regions where it had been elevated due to upwelling when there was no biology.

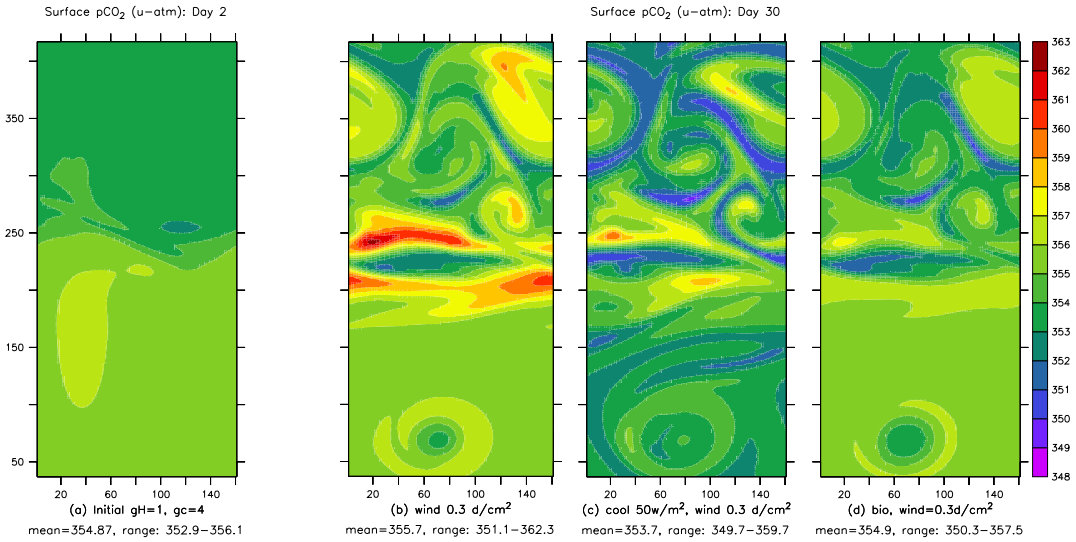


**Figure 4.** Surface $pCO_2$ in the model (a) on day 2, and (b)–(d) on day 30 of the simulation. These model runs were initialized with uniform $pCO_2$ at the surface and $\gamma = 4$ as shown in Fig. 1. An east-west wind stress of 0.3 dyne-cm$^{-2}$ was applied at the surface. Panel (b) shows the localized increase in surface $pCO_2$ that results from the upwelling of DIC, though this is somewhat offset by the lowered temperature. Panel (c) shows a decrease in surface $pCO_2$ within certain regions when the surface is cooled by a heat loss of 50 watts-m$^{-2}$. The reduction in $pCO_2$ is largest where the mixed layer depth is shallowest. Panel (d) shows the surface $pCO_2$ in a run with biological production that responds to the vertical flux of nitrate. The nitrate was initialized subsurface of 100 m using $\delta = 0.9$ which results in $\Gamma = 0.4$. The biological activity takes up most of the DIC upwelled and the $pCO_2$ enhancement seen in (b) is no longer seen in (d). The range of $pCO_2$ variations is only 11, 10 and 7 $\mu$-atm in each of these cases.

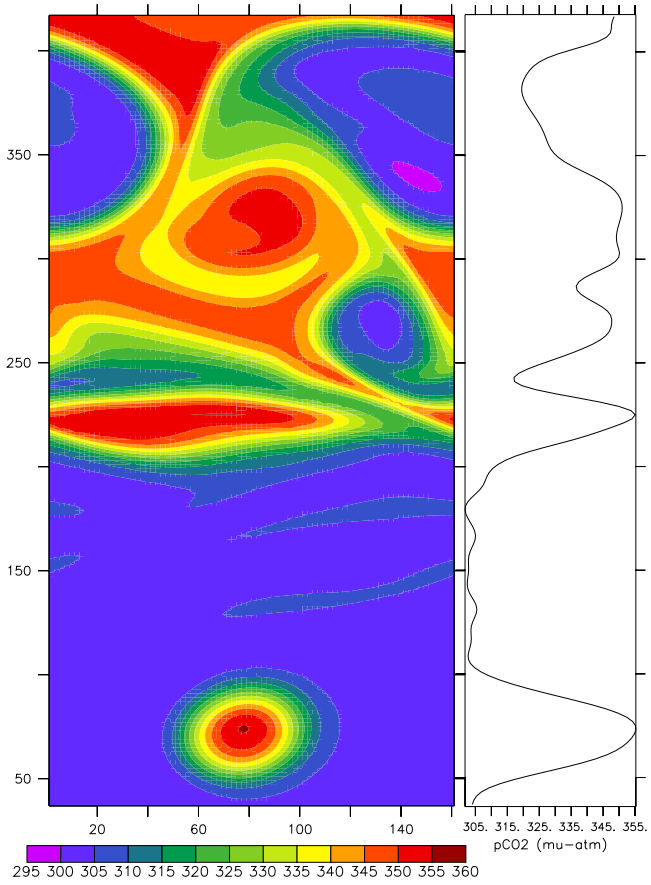


**Figure 5.** Surface $pCO_2$ on day 30 when the model is initialized with an across-front $pCO_2$ difference of approximately 60 $\mu$-atm ($\gamma_s = 0.5$). The ratio of vertical DIC and T gradients is the same as in previous runs ($\gamma = 4$), but the effect of upwelling on the surface $pCO_2$ field is undiscernable since it is dominated by the horizontal stirring of the different $pCO_2$ waters. The color scale is different than in Fig. 4. The variance in surface $pCO_2$ that initially exists at large scales, is converted to smaller scales by horizontal advection as the flow evolves. The magnitude of the $pCO_2$ variations remains more or less unaltered. This model run was performed with a heat loss of 50 watts $m^{-2}$, but in general, the effect of cooling and biological productivity in response to submeso-scale upwelling in undistinguishable in the surface $pCO_2$. The plot to the right shows the large surface $pCO_2$ variability along a mid-channel transect (at x= 80 km).